EXPERIMENTAL STUDY OF THE SHEAR ALFVEN

RESONANCE IN A TOKAMAK

by

FRANKLIN DOUGLAS WITHERSPOON

A thesis submitted in partial fulfillment of the

requirements for the degree of

Doctor of Philosophy

(Physics)

at the

UNIVERSITY OF WISCONSIN-MADISON

1984

ABSTRACT

EXPERIMENTAL STUDY OF THE SHEAR ALFVEN

RESONANCE IN A TOKAMAK

Franklin Douglas Witherspoon

Under the supervision of Professor Julien Clinton Sprott

Studies of a new rf heating technique in tokamaks, Shear Alfvén Resonance Heating, have been performed on the Tokapole II tokamak at the University of Wisconsin. High power heating experiments have been preceded by careful identification of the resonance and its properties at low power.

According to MHD theory, the shear Alfvén resonance manifests itself as a resonant enhancement of the wave magnetic field perpendicular to the equilibrium field at the location in the non-uniform plasma where the frequency, ω, and parallel wavelength match the Alfvén speed v_A, i.e. $\omega = k_{\parallel} v_A$. Experiments on the Tokapole II device have demonstrated the existence of the shear Alfvén resonance in a tokamak by direct probe measurement of the wave magnetic field within the plasma. The resonance is experimentally identified as a radially localized enhancement of the poloidal wave magnetic field. The radial location of the resonance agrees with a 2-D MHD

calculation which includes toroidicity and non-circularity of the plasma cross-section. Other properties of the resonance such as polarization, radial width, risetime to saturation, and resonant enhancement over the driving vacuum rf fields are found to be in good agreement with theory.

The resonances are driven by a novel launching structure which utilizes the four existing poloidal divertor rings within the vacuum vessel of Tokapole II. RF currents at ~1.2 MHz are driven through the mechanical supports of the divertor rings, and are superposed upon the transformer-induced equilibrium field shaping currents. Proper phasing of the currents in each ring allow approximation to poloidal mode numbers of m=1,2, or 4, and the toroidal structure of the antenna currents yields a step-wise approximation to toroidal mode numbers n=1 and 2. However, a broad n and m spectrum is generated.

These studies have provided the experimental base from which high power heating experiments utilizing the shear Alfvén resonance can be pursued.

Julian Clinton Sprott

MAY 3 1 1984

ACKNOWLEDGEMENTS

I would like to thank Professors J.C. Sprott and S.C. Prager for the support and advice they have given me throughout my graduate studies. I have also benefited from numerous discussions with Dr. C.E. Kieras and Professor J.A. Tataronis on the theoretical aspects of shear Alfvén heating of tokamaks. I especially want to thank Dr. Kieras for developing the numerical code which calculates the shear Alfvén resonance location in Tokapole II. I also would like to acknowledge the helpful advice and friendship of Professor R. Dexter.

A very special thanks goes to T. Lovell who kept Tokapole II going and without whose infinite patience and understanding this research would not have been possible. Special thanks also goes to my fellow graduate student D. Kortbawi who spent many a late night and weekend assisting in all facets of the experiment and who built, or assisted in building, much of the hardware. I wish him the best of luck in the future as he carries on with the experiment.

I have enjoyed working with all the graduate students in the UW plasma group but especially wish to thank the members of the Tokapole II group for their friendship and advice through the years: T. Osborne, D. Shepard, N. Brickhouse, A. Biddle,

D. Holly, T. Rempel, T. Leonard, M. Sengstacke and all the others.

I would also like to thank my parents Frank and Joyce Witherspoon and my brothers and sisters for their faith and support through the years.

Thanks go to my roommate and close friend of many years, Dr. Kevin Miller, and very special thanks go to my faithful dog Dora, who has put up with a lot of inattention and many late nights and yet still greeted me joyfully every time I returned home. She has been a joy in my life.

Last, but certainly not least, I wish to thank my fiancee, Margaret Daube, whose love and support over the past two years have kept me going when things were roughest.

Financial support was provided by the United States Department of Energy.

TABLE OF CONTENTS

CHAPTER 1

INTRODUCTION

It is sometimes the case that the dispersion relation which describes propagating waves in a uniform plasma, such as electrostatic plasma waves[1] or shear Alfvén waves[2], becomes a condition for a local resonance in a nonuniform plasma. If it can be arranged for an external antenna to match the mode structure and frequency of this resonance, then it may be possible to couple electromagnetic energy to the plasma from an external power source.

This theoretical result has been the cause of intensive research in the plasma physics community for many years. There are two primary reasons for this interest. First is the desire to understand the basic physics of the plasma state, for which waves are of fundamental importance. And secondly is the worldwide effort to produce a controlled fusion reactor.

The device which has received the most attention, and which is generally considered the closest to realization as a reactor, is the tokamak[3,4,5]. Like most other magnetic confinement devices, the basic tokamak design cannot reach ignition conditions on its own, but must rely on some form of auxiliary heating to supplement the ohmic heating of the toroidal current. Ohmic heating is insufficient because the

high conductivity of the plasma above a temperature of a few keV typically requires plasma currents which are larger than those allowed by MHD stability constraints. For non-tokamak devices such as mirrors and stellarators, supplementary heating must provide all the energy to reach ignition conditions.

The most successful auxiliary heating method to date has been injection of high energy neutral beams[6,7]. Unfortunately, this method has an uncertain future due to the technological complexity and expense of producing the high beam energies (>200 keV) that would be required for a reactor. At present, one of the most promising techniques for bringing tokamaks to ignition appears to be radio frequency (rf) heating. This method heats the plasma through the absorption, and subsequent thermalization, of electromagnetic wave energy which is generated by antennas near the plasma boundary. This is a versatile technique in that one can choose which class of particles the waves couple to, and in general the location in the plasma where the energy is deposited. The three most studied techniques have been Ion Cyclotron Resonance Heating (ICRH)[8,9], Electron Cyclotron Resonance Heating (ECRH)[10,11], and Lower Hybrid Heating (LHH)[12]. Each of these techniques has achieved some measure of success, with each having specific weaknesses and strengths. However, no single one of these has as yet proven itself as the method of choice for a tokamak

reactor. There is still plenty of room for, and interest in, new rf heating concepts.

This thesis will be concerned with one of the more promising of these new concepts, namely Shear Alfvén Resonance Heating (SARH). Although utilization of the shear Alfvén resonance for heating tokamaks was proposed more than ten years ago by Hasegawa and Chen[13] and Tataronis and Grossmann[14], it has only been in the last five years that experimental application of the technique to tokamaks has begun. There is currently a great deal of interest in this technique as promising new results appear. This is evidenced by the rapidly increasing number of both experimental and theoretical papers on SARH appearing in the literature and at plasma conferences during the past several years.

There are presently five experiments on SARH in tokamaks worldwide. The largest of these is on the TCA tokamak at Lausanne, Switzerland[15]. TCA is a medium sized tokamak built specifically to test SARH in a tokamak[16]. It has been operating since 1980 and has recently reported the first observation of ion and electron heating utilizing SARH in a tokamak[17]. Another experiment has been on the Pretext tokamak at the University of Texas, Austin[18]. They have concentrated on loading measurements with various antennas, and on CO_2 laser scattering experiments to observe wave phenomena. As of this writing, they have apparently observed the discrete global

Alfvén wave[19], but have yet to observe the shear resonance. Unfortunately, this experiment is being terminated. At the University of Wisconsin, Madison, we have concentrated on identifying the shear resonance directly through probe measurements[20], and are now involved in high power heating experiments[21]. Two other somewhat smaller experimental efforts are also underway on the Tortus tokamak at the University of Sidney, Australia[22] and in the RO-5 tokamak in the USSR[23]. Both have recently reported interesting results. Their experiments are only just beginning, however. Some earlier experiments were performed on a linear theta pinch[24] and in stellerator devices[25].

Just what are the features of SARH that have generated so much recent interest in this technique? Probably the single most appealing feature of SARH is its frequency range. A tokamak will probably need upwards of 100 MW of supplementary heating power to reach ignition. For the frequency range of SARH this is not a problem, involving essentially off-the-shelf technology. However, as the operating frequency regime for each technique rises, the technology to produce this power level becomes less available and more expensive. Table 1.1 puts SARH in context with the other three main rf heating methods.

A very appealing feature of SARH is that the energy is theoretically deposited on a magnetic flux surface, rather than

TABLE 1.1

	SARH	ICRH	LHH	ECRH
GENERATION				
frequency	1-2 MHz	50-100 MHz	1-5 GHz	50-200 GHz
sources	tubes	tubes	klystrons	gyrotrons
generation efficiency	90%	70%	60%	40%
attainable power per generator	10 MW	1-2 MW	1 MW	0.2 MW
TRANSMISSION				
method	coaxial line	coaxial line or ridged waveguide	waveguide	waveguide
power/line	10 MW	2 MW	1 MW	0.2 MW
COUPLING				
technique	loop antenna	loop antenna or cavity-backed aperture antenna	flush-mounted waveguide array with specified phases	flush-mounted waveguide array
mode-tracking?	no	maybe	no	no

in a cylindrical surface as for ICRH and ECRH. This feature could allow for the possibility of more uniform heating of the plasma, especially the plasma core. This feature could also provide a powerful method of profile modification through radially localized heating to adjust the local conductivity, current density, and temperature.

There is currently a great deal of interest in operating tokamaks in a steady state to eliminate the engineering problems associated with pulsed operation. Hasegawa[26], and Fisch and Karney[27] have suggested using Alfvén waves for current drive in a tokamak which could ultimately be as important as its heating function.

Unfortunately, there are also a few negative features associated with SARH. The most important of these is again more of a practical nature. Namely, the antenna requirements at lower frequencies seem to be more stringent. In principle, the lower frequencies would seem to require physically larger antennas. Since the mode that one is trying to drive in SARH is helical in nature, ideally one would then drive it with a helical antenna which wraps around the plasma current channel. This would be unfeasible for a reactor, since the antenna must be close to the edge of the plasma and shielding from the heat and neutron load would be a considerable problem. The solution appears to be to use several localized antennas somewhat similar to the antenna loops of ICRH. When properly located

and phased, coupling to the helical shear Alfvén mode would be possible. If efficient coupling can be attained with this technique then the antenna problem may turn out not to be any worse than that for ICRH. There are also other ideas for solving this problem, using different antenna designs, e.g. cavity resonators[28].

Other problems that may appear are enhanced radial transport induced by the rf fields and coupling to deleterious modes causing instabilities to occur. However, the recent heating results[17] from TCA have apparently not shown any degradation of confinement due to the rf and so these fears may turn out to be unfounded.

The experimental base for SARH in a tokamak is still in a very early stage of development with most of the theory, including that pertaining to the resonance itself, yet to be confirmed by experiment. This is quite similar to the state ICRH was in about 20 years ago when the basic concept had been established, but there existed little experimental data to confirm the theory. The shear Alfvén resonance has been directly observed in linear devices[29] and somewhat less directly in stellarators[30], but has not heretofore been observed in a tokamak.

The first most obvious question to ask about SARH in tokamaks from the outset, is whether the shear Alfvén resonance actually exists in a tokamak with the properties predicted by

MHD theory. If this most basic prediction of the theory were incorrect, then one could never hope to fully understand a heating experiment based on this theory. It thus seemed prudent to precede a high power heating experiment with careful identification of the resonance in a tokamak at lower power levels. With an identification firmly in hand, we could then confidently attack the heating experiment from a firm theoretical basis.

The resonance is most easily identified through its wave magnetic field inside the plasma, which is relatively straightforward to measure (for low temperature plasmas) and is a direct indicator of the resonance in the following sense. Since the resonance is an MHD resonance (i.e. predictable from MHD theory) we were guided in the design of the experiment primarily by MHD theory. According to MHD, three perturbation quantities are associated with the wave--the wave fluid velocity $\underline{\tilde{v}}$, magnetic field $\underline{\tilde{B}}$, and plasma pressure $\tilde{p}$. At the resonant location, where the drive frequency and mode structure of the external antenna provides a match to the local Alfvén velocity, $\underline{\tilde{v}}$ is predicted to be infinite, but this is not a readily measurable quantity in a plasma. $\underline{\tilde{B}}$ also becomes infinite and can be measured in Tokapole II with magnetic probes. The perturbed pressure of the wave is a somewhat indirect indicator of the resonance. If the equilibrium plasma pressure is zero (a good approximation for the low beta

Tokapole II plasma), MHD implies that $\tilde{p}$ is strictly zero everywhere. If the equilibrium pressure is nonzero, $\tilde{p}$ does blow up at the resonance, but much more weakly than $\underline{\tilde{B}}$. In fact, at the resonance $\tilde{p}/\tilde{B}$ goes to 0 even though $\tilde{p}$ and $\underline{\tilde{B}}$ both go to infinity. For typical measured values of $\tilde{B}$ in these experiments, $\tilde{p}/p < 10^{-4}$. Thus the plasma pressure is both indirect and difficult to measure. $\underline{\tilde{B}}$ is the observable of choice since it is both strongly divergent and measurable. This thesis will therefore concentrate almost exclusively on the magnetic field measurements of the resonance.

This thesis describes the initial experimental work performed for the Shear Alfvén Resonance Heating project at the University of Wisconsin. This is perceived as being a long-term research project with at least two follow-on theses. It is presently one of only two Alfvén heating programs in the United States, the other one being on the Pretext device at Texas. As of this writing, however, the experiment on Pretext appears to be in the final stages of being terminated.

In this thesis, we will describe measurements of the spatial and temporal properties of the resonance in a tokamak, and compare these results with MHD theory. In addition, the radial location of the resonance is compared with a two-dimensional calculation by Kieras and Tataronis[31,32] in which the ideal MHD equations are solved for the Tokapole II device, thereby including both toroidicity and noncircularity

of the plasma cross-section. We will show that, in all points, the measured resonance properties are consistent with those predicted by the theory. In doing this, we present what we believe to be a convincing case for the first direct observation of the shear Alfvén resonance in a tokamak.

In chapter 2 the basic theoretical model of the shear Alfvén wave in a non-uniform plasma is developed from MHD theory. Since kinetic effects are not critical to the results of this thesis, we give only cursory coverage to this topic. Finally, a brief summary of the analytical results obtained by Kieras and Tataronis for tokamaks and their numerical application to the Tokapole II device is presented.

Chapter 3 presents a description of Tokapole II and general machine hardware. The characteristics of typical plasma discharges are described along with the primary plasma diagnotics used.

A description of the rf apparatus used in this experiment is given in Chapter 4. This covers the launching structures, rf sources and magnetic probes. The two most difficult problems that had to be dealt with on a constant basis in this experiment were rf pickup on the diagnotics, especially on magnetic probes, and the struggle to construct probes that not only survived the discharge but that did not perturb the discharge significantly. This is also discussed in Chapter 4 which describes how these problems were eventually solved.

Chapter 5 presents the experimental data supporting the identification of the shear Alfvén resonance. The data are compared with the theoretical predictions from MHD, and the radial locations are shown to be in good agreement with the numerical calculations (of Kieras and Tataronis).

Chapter 6 summarizes the experimental results and makes suggestions for future experiments.

In this thesis, references will be made from time to time to PLP reports. These are internal papers of the University of Wisconsin Plasma Physics Group. Copies are available on request from:

Plasma Physics Department
University of Wisconsin
1150 University Ave.
Madison, WI 53706

REFERENCES - CHAPTER 1

1. E.M. Barston, Ann. Phys. 29, 282 (1964).

2. C. Uberoi, Phys. Fluids 15, 1673 (1972).

3. L.A. Artsimovich, Nucl. Fusion 2, 215 (1972).

4. H.P. Furth, Nucl. Fusion 15, 487 (1975).

5. J. Sheffield, Proc. IEEE 69, 885 (1981).

6. M.M. Menon, Proc. IEEE 69, 1012 (1981).

7. W. Stodiek, et al., IAEA-8, CN-38/A-1 (1980).

8. T.H. Stix, The Theory of Plasma Waves (McGraw-Hill, New York, 1962).

9. P.L. Colestock, C. Barnes, M. Bitter, D. Boyd, N. Bretz, et al., in Proceedings of the Fifth Topical Conference on Radio Frequency Plasma Heating (Madison, 1983).

10. R.M. Gilgenbach, et al., Phys. Rev. Lett. 44, 647 (1980).

11. C.P. Moeller, in Proceedings of the Fifth Topical Conference on Radio Frequency Plasma Heating (Madison, 1983).

12. T. Imai, T. Yamamoto, N. Suzuki, K. Uehara, et al., ibid.

13. A. Hasegawa and L. Chen, Phys. Rev. Lett. 32, 454 (1974); Phys. Fluids 17, 1399 (1974).

14. W. Grossmann and J. Tataronis, Z. Physik 261, 203 and 217 (1973).

15. A. DeChambrier, et al., Plasma Physics 24, 893 (1982); R. Keller, et al., in 4th Topical Conf. on RF Heating in Plasmas, (Austin, 1981).

16. A.D. Chettham, A. Heym, et al., CRPP Internal Report LRP 162/80, Lausanne (1980).

17. R. Behn, A. de Chambrier, et al., CRPP Internal Report LRP 232/83, Lausanne (1983).

18. D.W. Ross, et al., in 4th Topical Conf. on RF Heating in Plasmas, (Austin, 1981).

19. T.E. Evans, et al.; M.E. Oakes, et al.; and R.D. Bengtson, et al., Bull. Am. Phys. Soc. 28, 1085 (1983); R.D. Bengtson, et al., in 5th Topical Conf. on RF Heating in Plasmas, (Madison, 1983).

20. F.D. Witherspoon, et al., in 4th Topical Conf. on RF Heating in Plasmas, (Austin, 1981); S.C. Prager, et al., in 5th Topical Conf. on RF Heating in Plasmas, (Madison, 1983).

21. D. Kortbawi, F.D. Witherspoon, J.C. Sprott, and S.C. Prager, Bull. Am. Phys. Soc. 28, 1086 (1983).

22. R.C. Cross, et al., in Proc. 3rd Joint Varenna-Grenoble Int. Symp. Vol. I, 183 EUR7979EN (1982).

23. R.A. Demirkhanov, et al., in Proc. 9th Int. Conf. on Plasma Physics and Contr. Nucl. Fusion, (Baltimore, 1982).

24. R. Keller and A. Pochelon, Nucl. Fusion 18, 1051 (1978).

25. S.N. Golovato and J.L. Shohet, Phys. Fluids 21, 1421 (1978); K. Uo, et al., in Proc. 6th Int. Conf. on Plasma Phys. and Contr. Nucl. Fusion, IAEA-CN-37-L-1 (Berchtesgaden, 1976).

26. A. Hasegawa, Nucl. Fusion 20, 1158 (1980).

27. N. Fisch and C. Karney, Phys. Fluids 24, 27 (1981).

28. J.H. Mullen, Bull. Am. Phys. Soc. 28, 1043 (1983), F.P. Blau, S.C. Chiu, P.B. Parks, and J.M. Rawls, ibid., 1042.

29. A. Tsushima, Y. Amagishi, and M. Inutake, Phys. Letters 88A, 457 (1981).

30. S.N. Golovato and J.L. Shohet, Phys. Fluids 21, 1421 (1978).

31. C.E. Kieras, Ph.D. Thesis, University of Wisconsin (1982).

32. C.E. Kieras and J.A. Tataronis, J. Plasma Phys. 28, 395 (1982).

CHAPTER 2

THEORY

The existence of shear Alfvén waves in uniform plasmas has been well known for many years[1,2]. In a uniform plasma the Alfvén speed is constant, and the ideal MHD equations lead immediately to the dispersion relation for the propagation of small amplitude waves

$$\omega^2 = k_\parallel^2 v_A^2 = k_\parallel^2 B^2/\mu_o\rho$$

where $k_\parallel$ is the wave propagation vector and v_A is the Alfvén speed.

In nonuniform plasmas, such as those encountered in the laboratory, the Alfvén speed is no longer constant but is a function of position in the direction of the non-uniformity. In general there are non-uniformities in both density and magnetic field. Instead of a dispersion relation, the shear Alfvén wave now satisfies a resonance condition, where wave quantities $\to \infty$ and energy is absorbed at the location within the plasma where the frequency and parallel wave vector satisfy the local Alfvén speed, i.e.

$$\omega_o = k_\parallel v_A(x_o)$$

where x_o is the location where this condition is satisfied for the given ω_o and $k_\parallel$ which are usually specified by external oscillators and wave coupling structures.

The basic theoretical model for this resonance condition and its applicability to plasma heating was first suggested by Tataronis and Grossmann[3] and Hasegawa and Chen[4]. The first part of this chapter will follow Hasegawa and Chen in the derivation of the resonance condition. In the following sections we will follow Kappraff and Tataronis[5] to estimate the radial widths and risetimes of the resonances due to ohmic dissipation. We will then briefly discuss the "kinetic Alfvén wave" and some of its implications to heating. Finally, we will discuss toroidal effects in the MHD model following the work of Kieras and Tataronis[6,7]

a. Basic model

Following Hasegawa and Chen, we assume a one dimensional ideal MHD slab model with the non-uniformity in the x direction, i.e. the mass density ρ, pressure p, and equilibrium magnetic field $\underline{B}$ varying only as functions of x. The magnetic field is straight but has shear, i.e.

$$\underline{B}(x) = B_z(x)\hat{z} + B_y(x)\hat{y} \qquad (1)$$

Note that to extend these results to a toroidal plasma, x, y,

and z would correspond to the radial, poloidal, and toroidal directions respectively.

By linearizing the ideal MHD equations for small wave amplitudes, we are immediately led to the differential equation for the fluid displacement vector $\underline{\xi}$

$$\mu_o \rho \ddot{\underline{\xi}} - (\underline{B}\cdot\nabla)^2 \underline{\xi} = -\mu_o \nabla \tilde{p} - \underline{B}(\underline{B}\cdot\nabla)(\nabla\cdot\underline{\xi}) \qquad (2)$$

where $\tilde{p}=p+\underline{b}\cdot\underline{B}/\mu_o$ is the total pressure to 1st order, and $\underline{b}$ is the 1st order perturbation in the magnetic field. $\underline{b}$ and $\underline{\xi}$ are related through Maxwell's equations

$$\underline{b} = \nabla\times(\underline{\xi}\times\underline{B})$$

or

$$\underline{b} = (\underline{B}\cdot\nabla)\underline{\xi} - \underline{B}(\nabla\cdot\underline{\xi}) - (\underline{\xi}\cdot\nabla)\underline{B} \qquad (3)$$

To close the MHD equations we assume an adiabatic equation of state (not linearized yet)

$$\frac{d}{dt}(p\rho^{-\gamma}) = 0$$

Combining this with the continuity equation

$$\frac{\partial p}{\partial t} + \nabla\cdot(\rho\underline{v}) = 0$$

and linearizing yields the perturbed plasma pressure in terms of $\underline{\xi}$

$$\tilde{p} = -\xi_x \frac{dp}{dx} - \gamma p(\nabla\cdot\underline{\xi}) \qquad (4)$$

Fourier analyzing along the symmetry directions, y and z, but not along the non-uniformity direction, yields perturbations of the form

$$\underline{\xi} = \underline{\xi}(x)\exp[i(k_z z + k_y y - \omega t)] .$$

Let us define a more convenient set of local orthogonal rectangular coordinates:

$$\hat{e}_x = \hat{x}, \quad \hat{e}_\parallel = \underline{B}/B, \quad \hat{e}_\perp = \hat{e}_\parallel\times\hat{e}_x .$$

In this coordinate system, Eq. (2) becomes for each component

$$\varepsilon\xi_\parallel = ik_\parallel\mu_o\tilde{p} + iB^2k_\parallel(ik_\parallel\xi_\parallel + ik_\perp\xi_\perp + \frac{d\xi_x}{dx}) \qquad (5)$$

$$\varepsilon\xi_\perp = ik_\perp\mu_o\tilde{p} \qquad (6)$$

$$\varepsilon\xi_x = \mu_o\frac{d\tilde{p}}{dx} \qquad (7)$$

In these expressions, $\varepsilon(x) = \omega^2\mu_o\rho - k_\parallel^2B^2$, $k_\parallel(x)B(x) = k_zB_z +$

$k_y B_y$, and $k_\perp(x)B(x) = k_y B_z - k_z B_y$. By using Eqs. (3) and (4), $\xi_\perp(x)$ can be expressed in terms of $\xi_x(x)$ as

$$\xi_\perp(x) = \frac{i\alpha k_\perp B^2}{\alpha k_\perp^2 B^2 - \epsilon}\frac{d\xi_x}{dx} \qquad (8)$$

where

$$\alpha(x) = 1 + \gamma\beta\omega^2/(\omega^2 - \gamma\beta k_\parallel^2 v_A^2)$$

and

$$\beta(x) = \frac{p}{B^2/\mu_o}$$

For plasmas with low β (as for tokamaks like Tokapole II), $\gamma\beta<<1$ which implies $\omega_o^2 >> \gamma\beta k_\parallel^2 v_A^2$, and we thus have $\alpha(x) = 1+\gamma\beta \sim O(1)$. Substitution of Eqs. (6) and (8) then leads to the wave equation for ξ_x

$$\frac{d}{dx}\left(\frac{\epsilon\alpha B^2}{\alpha k_\perp^2 B^2 - \epsilon}\frac{d\xi_x}{dx}\right) - \epsilon\xi_x = 0 \qquad (9)$$

Note that if the non-uniformity is removed, $\frac{d}{dx} \to 0$, and (9) reduces to

$$\epsilon\xi_x = 0$$

or

$$(\omega^2\mu_o\rho - k_\parallel^2 B^2)\xi_x = 0 \qquad (10)$$

thus recovering the shear Alfvén wave in a uniform plasma. The compressional wave is recovered by letting $\frac{d}{dx} \to ik_x$, which immediately yields the dispersion relation for the compressional Alfvén wave,

$$\omega^2 = k^2 v_A^2 .$$

Eq. (9) has a singular solution when the leading coefficient is zero. This occurs at the location $x=x_o$ where $\epsilon=0$, i.e. when $\omega = k_\parallel v_A(x)$. Near $x=x_o$

$$\epsilon(x) = \left(\frac{d\epsilon_r}{dx}\right)_{x_o}(x-x_o)$$

where ϵ_r is the real component of ϵ. (An artificial dissipation can be included in the analysis by including a small imaginary component, ϵ_i in ϵ.) Using this Taylor expansion of $\epsilon(x)$ to evaluate Eq. (9) near $x=x_o$ yields

$$\frac{d^2\xi_x}{dx^2} + \frac{1}{x-x_o}\frac{d\xi_x}{dx} - k_\perp^2\xi_x = 0 \qquad (11)$$

The approximate solution for ξ displays a logarithmic singularity near $x=x_o$.

$$\xi_x = C\ \ln(x-x_o). \qquad (12)$$

We are also interested in determining the behavior of the

other perturbation wave fields near the resonance. Specifically, we are interested in determining b_x, $b_\perp$, $b_\parallel$ near the resonance. We can then compare experimental measurements with these predictions.

In the low β limit $\hat{p} = \underline{b}\cdot\underline{B}/\mu_o$. Thus Eq. (7) can be rewritten as

$$\varepsilon\xi_x = \mu_o \frac{d}{dx}(\underline{b}\cdot\underline{B}/\mu_o)$$

$$= \frac{d}{dx}(b_\parallel B) = Bb_\parallel' \ .$$

Near the resonance, $\xi_x \sim \ln(x-x_o)$ which diverges, but $\varepsilon \sim (x-x_o)$. Since $(x-x_o)\ln(x-x_o) \to 0$ as $x \to x_o$ this implies that $b_\parallel' = 0$, and thus that $b_\parallel$ = constant.

Next, Eq. (6) can be written as

$$\varepsilon\xi_\perp = ik_\perp b_\parallel B$$

Thus

$$\xi_\perp(\omega) = ik_\perp b_\parallel B/\varepsilon \sim \frac{1}{x-x_o(\omega)} \ .$$

Taking the x-component of Eq. (3) yields

$$b_x = ik_\parallel B\xi_x \sim \ln(x-x_o)$$

And finally taking the $\perp$-component of Eq. (3) yields

$$b_\perp = iBk_\parallel\xi_\perp \sim \frac{1}{x-x_o(\omega)}$$

Even though we have now determined all the fields, for completeness we would also like to determine the behavior of $\xi_\parallel$ at the resonance. To do this look at the force balance equation

$$\rho\frac{d\underline{v}}{dt} = \underline{J}\times\underline{B} - \nabla p$$

Taking the parallel component of this equation we obtain

$$\rho\frac{dv_\parallel}{dt} = 0$$

or

$$\omega^2\rho\xi_\parallel = 0$$

since the terms on the right hand side are all $\perp$ to the equilibrium field.

To summarize the wave field behavior at the resonance, we have

$$\xi_{\parallel} = 0$$

$$\xi_{\perp} \sim \frac{1}{x-x_o(\omega)}$$

$$\xi_x \sim \ln(x-x_o(\omega))$$

$$b_{\parallel} \sim \text{constant}$$

$$b_{\perp} \sim \frac{1}{x-x_o(\omega)}$$

$$b_x \sim \ln(x-x_o(\omega))$$

All the quantities we have been dealing with so far, i.e. $\underline{\xi}$ and $\underline{b}$ are the transform variables in frequency space. To determine the time behavior of these quantities, we must perform an inverse Laplace transform. This has been done by Tataronis[9], assuming a forcing function to represent an external coupler at a driving frequency of ω_o. This yields the following time behavior for the fields:

$$b_{\parallel}(t) \sim \sin \omega_o t$$

$$b_{\perp}(t) \sim t \sin\omega_o t$$

$$b_x(t) \sim \ln t \sin\omega_o t \ .$$

We thus see that the wave magnetic field parallel to the equilibrium field simply oscillates and does not grow in amplitude. Both the radial component and the perpendicular component (which lies in a flux surface for a tokamak) are divergent in time with the perpendicular component being more strongly divergent than the radial component. It is the perpendicular component of the wave field that is studied experimentally in this thesis.

In the same paper, Tataronis calculates the energy absorption rate for ideal MHD by taking the dot product of $\underline{v}$ with the linearized momentum conservation equation and then integrating over the plasma volume, forming thus an energy equation for ideal MHD. The resulting expression is

$$W = \frac{2\pi L_y}{k}\int_0^a dx \left\{ \frac{1}{2}\rho(x)\underline{v}^2(x,t) + \frac{1}{2\mu_o}k^2B^2(x)\underline{\xi}^2(x,t) \right\}. \qquad (13)$$

where L_y is the plasma extent in the y direction, a corresponds to the radius of the plasma (the x-direction) and the integral along the z-direction extends for one wavelength in the z-direction, and $\underline{v} = \frac{d\underline{\xi}}{dt}$. The first term represents the wave

kinetic energy while the second term represents a wave potential energy.

Since the perpendicular components of the wave fields are non-square integrable, the wave energy grows without bound, accumulating in an infinitesimally narrow region about the singular surface. The fields away from the resonant surface simply oscillate at constant amplitude while those at the resonant surface grow in time. For a real plasma, dissipative processes should be considered. However, before discussing that, let us digress briefly to make a connection with experiment.

The design of a coupling structure which can drive these resonant modes can be qualitatively understood from the screw-pinch model. The resonance occurs when $\varepsilon = 0$, i.e. when

$$\omega^2(r) = (\underline{k}\cdot\underline{v}_A)^2$$

or

$$\omega^2(r) = (k_z B_z + k_\theta B_\theta)^2/\mu_o\rho$$

where again z and θ are the axial and azimuthal directions, respectively and r is the minor radius. To make the connection to a tokamak, this expression can be rewritten as

$$\omega^2(r) = (n + \frac{m}{q})^2 B_z^2/\mu_o\rho R^2 \qquad (14)$$

where q is the safety factor, rB_z/RB_θ, R is the major radius and n and m are the toroidal and poloidal mode numbers respectively. The approximations $k_z = k_\zeta = n/R$ and $k_\theta = m/r$ have been made. In general, the coupling structure should have the same toroidal and poloidal mode structure as the resonant mode, covering as large a fraction of the plasma surface area as is physically possible. Ideally, sheet currents which completely enclose the plasma are the best, and many theoretical calculations assume just such a current distribution[9,10,11]. In reality, such current distributions can be approximated by line currents which wind around the plasma cross-section in a helical fashion (see Figure 4-1). By choosing toroidal and poloidal mode numbers of opposite sign, it is possible to obtain resonant frequencies that are quite low. This is one of the more interesting aspects of SARH from a practical point of view, since it allows for the possibility of heating at the relatively low frequency range of ~ 1 MHz, for which a mature rf technology exists.

b. Dissipation

In the ideal MHD model, as time $t \to \infty$ the wave fields grow indefinitely and the resonance width, Δ, approaches zero. In a real plasma, dissipation of the wave fields by the plasma will

keep $\underline{b}$ and Δ finite. A resistive MHD boundary layer calculation has been performed by Kappraff and Tataronis[5] in which resistivity η was included in a thin layer about the resonant surface and assuming ideal MHD outside this thin layer, with the solutions in the two regions matched at the boundary.

Their analysis revealed two time scales which characterize the energy absorption process. Up to some critical time, τ_{rise}, which scales as $\eta^{-1/3}$, the incoming energy accumulates about the resonant surface just as in the ideal MHD case. This scaling is a result of matching solutions at the boundaries between the resistive layer and the surrounding ideal regions. For times greater than this, the growing resonant wave fields in the resistive layer have saturated in amplitude and the incoming energy is transferred to heat through ohmic heating of the electrons. The idea is illustrated in Figure 2-1, which comes from their paper.

The expression they derived for the time to saturate is

$$\tau_{rise} \approx \left(\frac{24\mu_o}{\omega_o^2 \eta}\right)^{1/3} \left(2\frac{B'}{B} - \frac{\rho'}{\rho}\right)^{-2/3} \qquad (15)$$

where the prime indicates derivatives with respect to the non-uniformity direction x, and all quantities are evaluated at the singular surface $x=x_o$.

To lowest order in the resistivity, they found the rate of

Fig 2-1. Growth of the wave fields in the ideal and resistive MHD cases.

WITH ABSORPTION

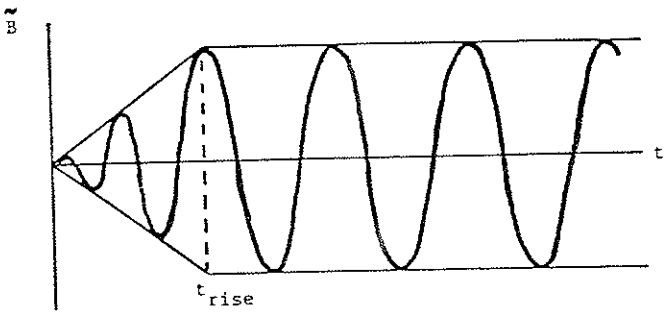

IDEAL MHD

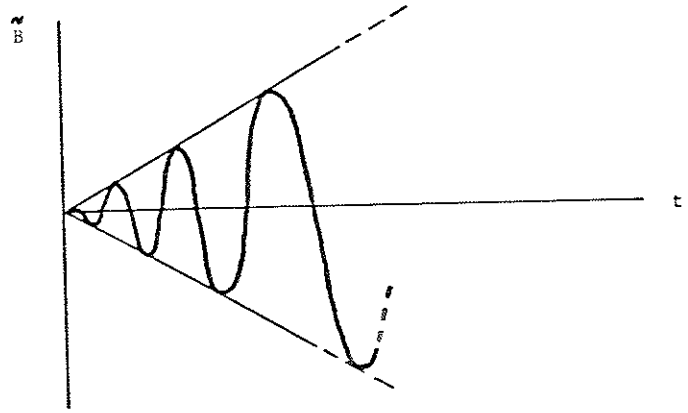

absorption to be equal to that of the ideal MHD case. An estimate of the resistive width can then be obtained by formally setting the heating rate due to ohmic heating (integrated around some small layer of width Δx) to the ideal MHD heating rate as calculated in Tataronis[8]. In other words,

$$\int_{plasma} \eta j^2 dx = \left(\frac{dW}{dt}\right)_{ideal\ MHD}$$

Assuming a constant η in the resistive layer and $\eta=0$ everywhere else, the following estimate for the resistive width was obtained

$$\Delta x \approx .8\pi \left(\frac{\eta}{\mu_o \omega_o}\right)^{1/3} \left(2\frac{B'}{B} - \frac{\rho'}{\rho}\right)^{-1/3} \qquad (16)$$

We will use these expressions in Chapter 5 to estimate the predicted radial width and risetime of the observed resonances.

c. Kinetic effects

In order to obtain a more realistic picture of the resonance in a collisionless plasma, such as would be encountered in a reactor, effects due to electron inertia, finite ion gyroradius, and dissipative processes such as ion viscosity, electron collisions, Landau damping, and nonlinear

processes must be included. This has been done by Hasegawa and Chen[12] and Ross[10].

When the perpendicular wavelength $2\pi/k_\perp$ becomes comparable in magnitude to the ion gyroradius, ρ_i, ions can no longer be considered tied to the field lines, whereas the lighter electrons are still tied. Wave motion thus induces a charge separation and a coupling to the electrostatic mode. Including these effects leads to the kinetic Alfvén wave, whose dispersion relation is given by

$$\omega^2 = k_z^2 v_A^2 [1 + k_\perp^2 \rho_i^2 (\tfrac{3}{4} + \tfrac{T_e}{T_i})] .$$

Due to the small $k_\perp$ this kinetic Alfvén wave can propagate across the magnetic field and can be dissipated by both electron and ion Landau damping on the $E_\parallel$ associated with the wave. (There is no $E_\parallel$ in the ideal MHD case since no charge separation arises.) This dispersion relation holds for $v_{T_e} > v_A$. If the opposite is true, then the dispersion relation must be modified to

$$\omega^2 = k_z^2 v_A^2 (1 + k_\perp^2 \rho_i^2)\left(1 + \frac{k_\perp^2 c^2}{\omega_{pe}^2}\right)^{-1}$$

The physical importance of this is that for $\beta < m_e/m_i$ (or equivalently $v_{T_e} < v_A$), where $\beta = p/(B^2/\mu_o)$ is the plasma beta, the kinetic wave will propagate to the lower density side of

the mode conversion surface. In a tokamak this would be towards the plasma edge, thus causing edge heating, which is not desired. For $\beta > m_e/m_i$, the wave propagates to the higher density side and can thus heat the plasma core. If the damping rate of the wave as it spirals in towards the core is such that it completely damps away by the time it reaches the center, then this process could provide a very uniform method of heating the plasma core. If the damping rate is very fast (relative to plasma scale lengths) then the wave energy will be deposited closer to the mode conversion surface, in which case it could provide not only heating, but also provide a means of modifying plasma profiles through local adjustments of the temperature and conductivity.

The singular surface of ideal MHD is removed by the non-ideal effects. However, the qualitative processes of the wave are similar, with only the addition of a large k_x (wave vector in the radial direction). The singular surface is replaced by a mode conversion layer where the incoming wave, from the external coupler, is converted into the kinetic Alfvén wave which then spirals into the plasma core. Hasegawa and Chen have shown that as long as the wave is completely damped before reaching the center of the plasma (no wave reflection), then the absorption is the same as that calculated for the ideal MHD case.[12]

Hasegawa and Chen also calculate the wave fields assuming

some given source term, which represents the external coupler. They find that the poloidal wave field at the mode conversion layer is enhanced over the corresponding vacuum wave field from the coupler. The enhancement factor is given by the expression

$$|B_{pol}| \sim (\kappa\rho_i)^{-2/3}[1 + (T_e/T_i)k_x^2\rho_i^2]\ |B_{pol\ vac}| \qquad (17)$$

where $B_{pol\ vac}$ is the vacuum wave field strength produced by the external antenna. For a reactor, where $\kappa \sim r^{-1} \sim 10^{-3}\rho_i^{-1}$, this enhancement can be as large as 100. For Tokapole II it is somewhat less as will be seen in Chapter 5.

As a final point to consider in this section, we can also make some rough estimates of the width of the resonance due to ion viscosity and electron Landau damping. Hasegawa and Chen[12] give expressions for the heating rates due to ohmic heating, ion viscosity, and electron Landau damping. Arguing heuristically that the width should scale as the heating rate to the 1/3 power, as Tataronis found for the resistive MHD case (since heating rate $\sim \eta$), we calculate the ratios of heating rates of ion viscosity and electron Landau damping to the ohmic heating rate. For ion viscosity we get

$$\frac{(dW/dt)_{ion\ viscous}}{(dW/dt)_{ohmic}} \sim \left(\frac{m_i}{m_e}\right)^{1/2} \left(\frac{T_i}{T_e}\right)^{3/2} \frac{1}{\beta_i} \qquad (18)$$

where $\beta_i = 2v_{T_i}^2/v_A^2$.

For electron Landau damping (ELD) we get

$$\frac{(dW/dt)_{ELD}}{(dW/dt)_{ohmic}} \sim \frac{\omega\nu_{ei}}{\delta_e k_z^2 v_{T_e}^2} \qquad (19)$$

We will make use of these expressions in Chapter 5.

d. Toroidal effects

It is not clear a priori that the results of the screw-pinch model are immediately applicable to the case of a tokamak for the following reason. The screw-pinch model has two degrees of symmetry, the axial and the azimuthal directions. All quantities are functions only of the radius r. This means, in particular, that the resonance condition given by Eq. (11) is satisfied, for ω_o, at a given radius $r = r_o(\omega_o)$. A resonant surface has constant radius and is thus also a magnetic surface. Each surface has a different resonant frequency, given by Eq. (11), thus giving rise to a continuous spectrum of frequencies. This simple resonance condition breaks down in a tokamak because surfaces of constant $k_\parallel v_A$ do not coincide with a magnetic surface due to the 1/R dependence of the toroidal magnetic field. Estimates for the shear Alfvén continuum frequencies in a tokamak based on the screw-pinch approximation may not, therefore, be particularly accurate.

Pao[13] and Goedbloed[14] were the first to treat the toroidal problem. They showed that by expressing the MHD equations in

the natural orthogonal flux coordinates of a toroidal system, that the continuum in an axisymmetric tokamak is determined by the eigenvalues of a set of coupled first order ordinary differential equations on each flux surface. It turns out that even though v_A is not constant on a flux surface, the eigenvalues are discrete on a given flux surface and cover a continuous range as the flux surface is varied from the magnetic axis out to the plasma edge. The radial eigenfunction can be shown to be singular on the resonant surface ψ_o, where $\omega_o^2 = \omega_A^2(\psi_o)$. This problem has also been treated by Tataronis, Talmadge and Shohet[15], Tataronis and Salat[16], Hameiri[17], and Hameiri and Hammer[18] for more general toroidal equilibria (for instance stellerators). None of these studies derived analytical expressions for the continua in a toroidal equilibrium.

Kieras[6,7] has taken this one step further by deriving analytic expressions for the shear Alfvén continuum for a large aspect ratio tokamak by solving the set of coupled differential equations on each flux surface. Toroidicity is included as a perturbation in the calculation utilizing an expansion in terms of the inverse aspect ratio $\varepsilon=a/R_o$, where a is the minor radius and R_o is the major radius of the plasma. The set of equations is then solved numerically. Specification of the equilibrium is provided by a numerical code[19] which solves the Grad-Shafranov equation in the poloidal divertor configuration

of Tokapole II, thereby including effects due to non-circularity of the plasma cross-section.

Kieras found that, to lowest order in this expansion, the continuum is given approximately by the continuum of the corresponding screw-pinch model. However, first order corrections due to the toroidicity cause a coupling between particular poloidal modes on rational q surfaces. Because of this coupling, gaps can form in the spectrum in which there are no continuum modes. (Chance and Cheng[20] have recently indicated the possibility of low toroidal number discrete modes occurring in the gap.)

This mode coupling can be explained by the following picture. In the simple screw-pinch model, it is possible for degeneracies to occur in the solution of the spectrum. This happens because on a given magnetic surface two different modes can have the same parallel wave number $k_\parallel = (m - nq)/r$ and hence the same resonant frequency. This is illustrated in Figure 2-2 where the degeneracy occurs at the q=3/2 surface.

The degeneracy in the cylindrical case is removed by the toroidal perturbation as illustrated in Figure 2-3. Here, the dashed curve represents the radial dependence of the resonant frequency for a cylinder showing the degeneracy of the (m,n) = (2,2) and (3,2) modes. The solid curves represent the solution with toroidicity included. The degeneracy is removed by a coupling or mixing of the two modes forming a gap in the

Fig. 2-2. Degeneracy in the cylindrical model occurs when two modes have the same $k_{\parallel}$. For the case shown, degeneracy occurs at the q = 3/2 surface.

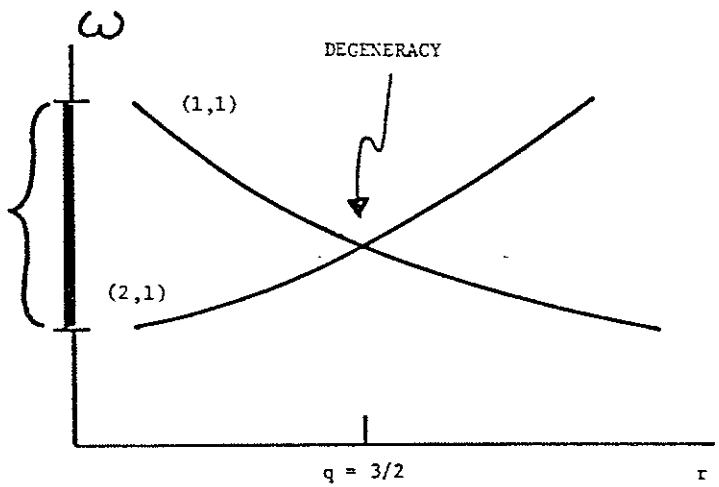

$$k_{\parallel} \sim m - nq$$

Thus

$$k_{\parallel}|_{(1,1)} \sim 1 - \frac{3}{2} = -\frac{1}{2} \qquad \text{at} \quad q = \frac{3}{2}$$

$$k_{\parallel}|_{(2,1)} \sim 2 - \frac{3}{2} = \frac{1}{2} \qquad \text{at} \quad q = \frac{3}{2}$$

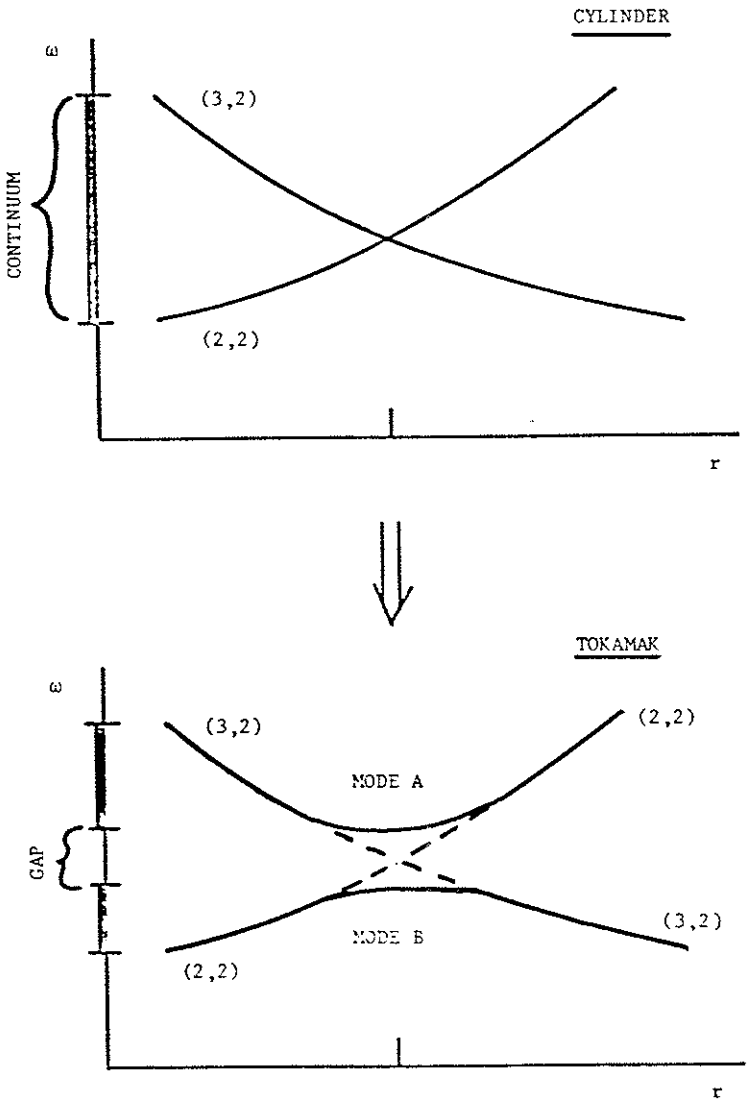

Fig. 2-3. Removal of the degeneracy in a cylinder by toroidal effects causing mode coupling between poloidal modes with same toroidal mode number.

frequency spectrum in which no resonance exists. The reason for the gap is revealed through the poloidal structure of the two modes, labelled A and B in the figure. At radii far from the mode coupling surface (where the degeneracy had existed) mode A is nearly a pure m=3 mode on the inside or a pure m=2 mode on the outside (of the torus). The mode labelled B is just the opposite. Right at the mode-coupling surface both modes A and B are a mixture of m=2 and m=3 modes as shown in Figure 2-4. In fact, modes A and B have identical structures there except for being shifted 180° in poloidal angle. Mode A peaks in the high field, high v_A, inner region of the torus and thus has a higher resonant frequency than the mode B which peaks in the low field, low v_A, outer region of the torus.

Kieras points out that this gap which forms due to coupling of degenerate poloidal modes is analogous to the gap which forms in the energy spectrum of electrons in a periodic crystal lattice. For that case, gaps form because of wave localization in either the high or low potentials in the regions near or in between the ion lattice sites. Similarly, gaps form in the Alfvén spectrum because of mode coupling between poloidal modes which tends to localize the eigenfunctions in regions of high and low Alfvén velocity corresponding to the high or low field regions of the toroid.

The importance of this gap formation is that it predicts that at certain oscillator frequencies and antenna mode

Fig. 2-4: Poloidal mode structure of coupled modes at mode coupling surface shows a mixing of the poloidal modes.

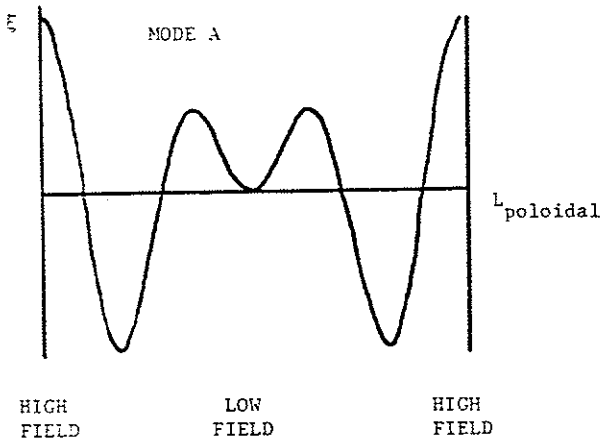

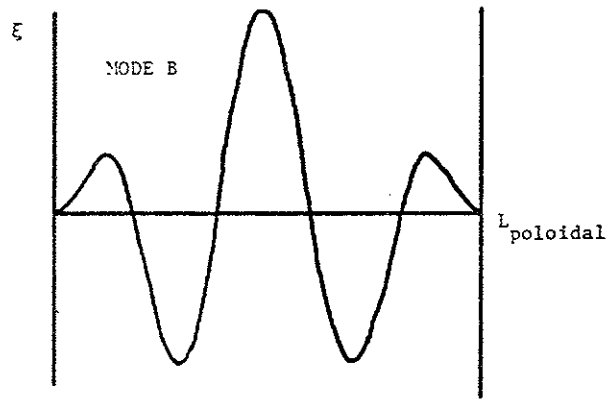

structures (helicities) it may not be possible to heat the plasma.

For further details concerning the analytical and numerical work of Kieras, the interested reader is directed to references 6 and 7.

REFERENCES - CHAPTER 2

1. A. Hasegawa and C. Uberoi, The Alfven Wave, Technical Information Center, USDOE (1982).

2. T.H. Stix, The Theory of Plasma Waves (McGraw-Hill, New York, 1962), Chapters 1 and 2.

3. W. Grossmann and J. Tataronis, Z. Physik 261, 203 and 217 (1973).

4. A. Hasegawa and L. Chen, Phys. Rev. Lett. 32, 454 (1974); Phys. Fluids 17, 1399 (1974).

5. J.M. Kappraff and J.A. Tataronis, J. Plasma Phy. 18, 209 (1977).

6. C.E. Kieras, Ph.D. Thesis, University of Wisconsin (1982).

7. C.E. Kieras and J.A. Tataronis, J. Plasma Phys. 28, 395 (1982).

8. J.A. Tataronis, J. Plasma Phys. 13, 87 (1975).

9. J.A. Tataronis and W. Grossmann, Nucl. Fusion 16, 667 (1976).

10. D.W. Ross, G.L. Chen, and S.M. Mahajan, Phys. Fluids 25, 652 (1982).

11. J.A. Tataronis and W. Grossmann, Courant Institute of Mathematical Sciences, NYU, Report MF-84, COO-3077-102 (1977).

12. A. Hasegawa and L. Chen, Phys. Fluids 19, 1924 (1976).

13. Y.P. Pao, Nucl. Fusion 15, 631 (1975).

14. J.P. Goedbloed, Phys. Fluids 18, 1258 (1975).

15. J.A. Tataronis, J.N. Talmadge, and J.L. Shohet, Proc. 3rd Topical Conf. on RF Plasma Heating, (Pasadena, 1978), also Comments Plasma Phys. Controlled Fusion 7, 29 (1982).

16. J.A. Tataronis and A. Salat, Proc. 2nd Joint Grenoble-Varenna Int. Symp. on Heating in Toroidal Plasmas, (Como, Italy, 1980).

17. E. Hameiri, Phys. Fluids 24, 562 (1981).

18. E. Hameiri and J.H. Hammer, Phys. Fluids 22, 1700 (1979).

19. M.W. Phillips, University of Wisconsin PLP 765 (1978).

20. M.S. Chance and C.Z. Cheng, Sherwood Theory Conference, paper 1P10 (1984).

CHAPTER 3

TOKAPOLE II

3.A. Machine description

The experiments described in this thesis were performed on the Tokapole II device at the University of Wisconsin[1]. Tokapole II (Figure 3-1) is a small tokamak which operates in a four-node poloidal divertor configuration which is formed by four internal field shaping rings. More complete descriptions of the device can be found elsewhere[2,3].

The vacuum vessel is an aluminum torus with a major radius of 50 cm and a square cross-section 44 cm on a side (Figure 3-2). Since field soak-in time for the 3 cm thick aluminum wall is about 15 msec, insulated gaps in both the toroidal and poloidal directions are provided in order to allow the magnetic fields to enter the machine. Vacuum is maintained by a 1500 l/sec turbomolecular-pump, which typically yields base pressures of low 10^{-7} Torr when the system is clean and relatively leak-free. Both Taylor[4] and glow discharge[5] cleaning have been used to condition the walls overnight and after bringing the system up to atmospheric pressure.

The field shaping rings are located at the four corners of the vacuum vessel (Figure 3-2). Each ring is made of a high conductivity chromium-copper alloy with a minor cross-sectional

Fig. 3-1. Tokapole II.

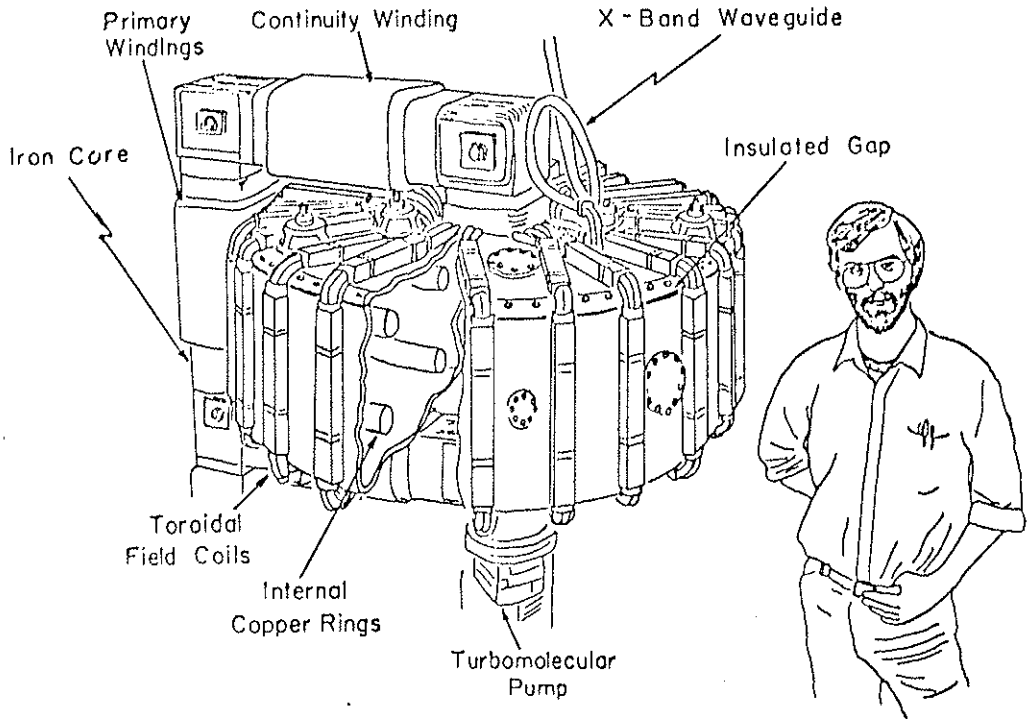

TOKAPOLE II

Fig. 3-2: Cross section of vacuum vessel showing internal rings.

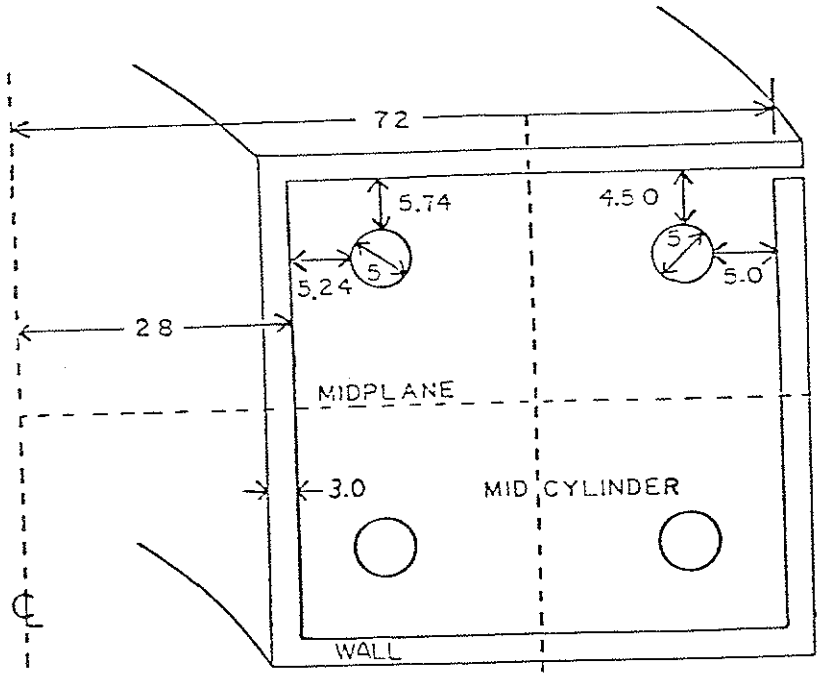

DIMENSIONS IN cm

diameter of 5 cm. Each ring is supported by three, equally spaced, high strength, beryllium-copper rods which are in turn electrically insulated from the vacuum vessel walls. The field shaping rings can be vertically adjusted ±5 mm without breaking vacuum to position the plasma.

The toroidal magnetic field, B_t, is produced by a 96 turn poloidal winding. This winding is energized by a 52 mF, 5 kV capacitor bank which is switched through a class E ignitron. The quarter period of this circuit is ~10 msec with the field passively crowbarred at peak field strength. This provides a nearly constant field for the major part of the discharge. When fully charged, this system will produce ~8 kG on the machine axis. However, due to the mechanical and electrical stresses of such high fields, the machine is normally run in the 2-6 kG range. All of the experiments described here were performed in this range.

The toroidal plasma current, I_p, and the divertor currents, I_h, in the field shaping rings are both induced by the transformer action of an iron core. The core has a flux swing capability of 0.15 webers and is usually reverse-biased ("cocked") in order to keep the core from saturating during a plasma discharge. The transformer core primary windings are driven by a 7.2 mF, 5 kV capacitor bank also switched through a class E ignitron. The 40:1 turns ratio yields a half period of ~5.6 msec. An 80:1 turns ratio is also available but not used

for these experiments. A 0.96 F, 450 V capacitor bank provides a "power" crowbar capability which clamps the poloidal gap voltage, V_{pg}, to a few volts, thus extending the discharge duration.

The poloidal field, B_p, is a superposition of the field produced by the toroidal plasma current and the vacuum octupole field generated by the four ring currents. Since these currents are in the same toroidal direction, there will be nulls (x-points) in the poloidal field located between the central plasma current channel and each of the four rings. The vacuum poloidal magnetic field is shown in Figure 3-3a, and the corresponding theoretical flux plot for a case with plasma current is shown in Figure 3-3b. Both square and dee-shaped equilibria can be produced as measured by magnetic probes[6,7]. The location of the x-points depends on the ring positions and the ratio of the plasma current to the ring currents and can be varied experimentally over a several centimeter range. The dotted line is the separatrix which represents the boundary between field lines which encircle one or more of the rings and field lines which encircle only the central plasma current channel. The plasma current is typically 10-20% of the total ring current.

The theoretical flux plot shown above assumes no plasma current flows outside the separatrix, whereas in reality roughly one-third of the total plasma current can flow in the

Fig. 3-3a: Poloidal magnetic flux plot in vacuum.

Fig. 3-3b: Poloidal magnetic flux plot with plasma.

CONTOURS OF POLOIDAL MAGNETIC FLUX

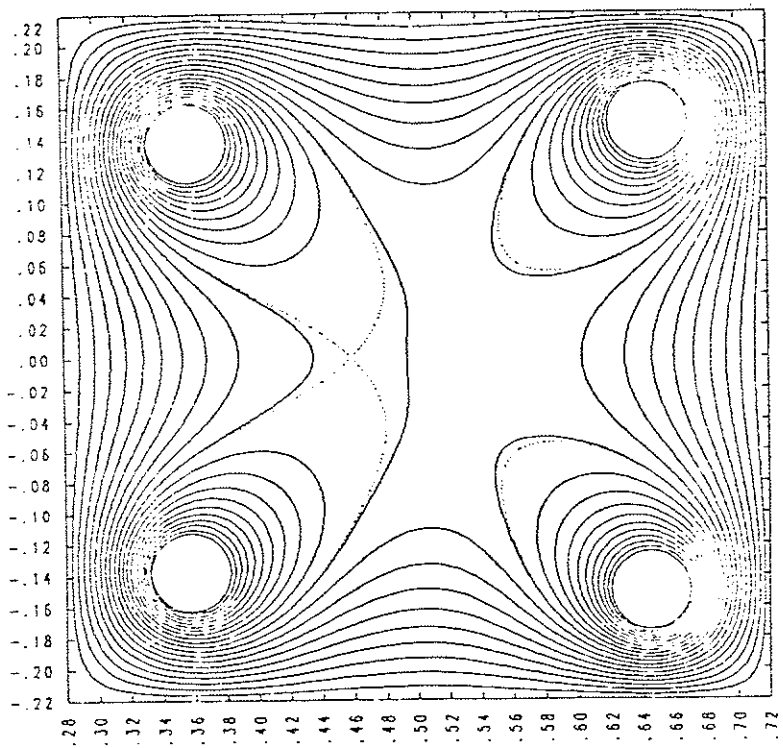

CONTOURS OF POLOIDAL MAGNETIC FLUX

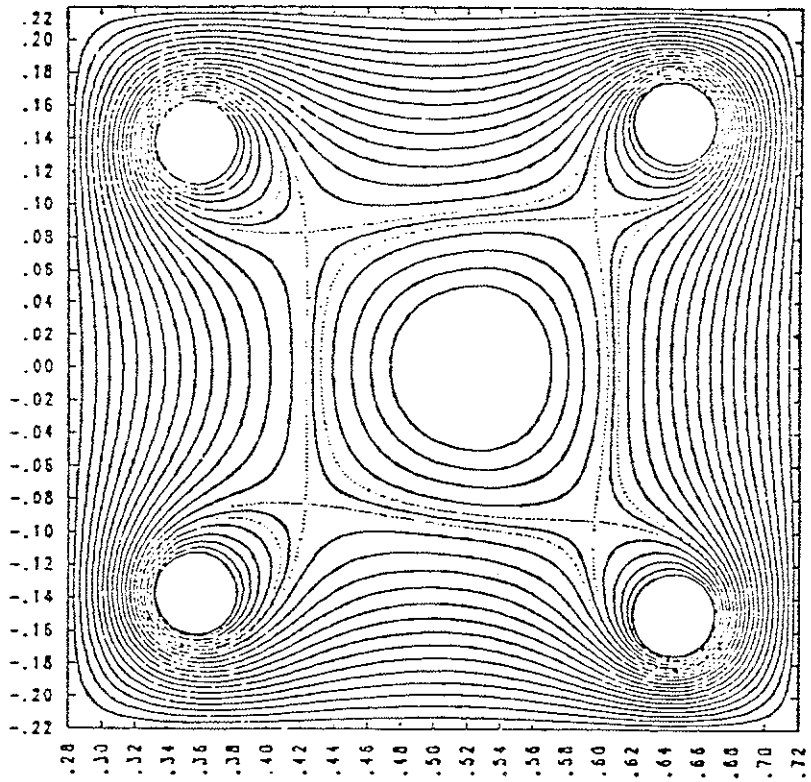

common-flux region. Stainless steel scrape-off plates can be extended up to the separatrix from all four sides at one toroidal azimuth. These "baffles" intercept field lines in the "divertor scrape-off region" and prevent current from flowing. Most of the experimental work of this thesis was done with the baffles inserted. Figure 3-4 shows the scrape-off plates and definitions for future reference.

A number of probe ports are scattered around the machine to facilitate diagnostic access to the plasma. These ports allow insertion of a wide variety of probes and diagnostics into the machine while maintaining the vessel under vacuum throughout the process.

4.B. Plasma Characteristics

Plasma formation in Tokapole II is basically the same as in all other tokamaks, and has been described in detail by Groebner[3]. For further information concerning tokamaks in general the interested reader is directed to the several review articles covering the subject[8,9,10].

The time evolution of a Tokapole II discharge is indicated schematically in Figure 3-5. A fast piezoelectric "puff" valve is triggered 16.66 msec before the poloidal gap voltage, V_{pg}, is applied, allowing hydrogen gas to fill the vacuum chamber to a pressure of typically 100-500 mTorr. The toroidal field is passively crowbarred at its peak value to provide an

Fig. 3-4: Central current channel is separated from the outer scrape-off (common flux) region by the separatrix. Stainless steel limiter plates can be inserted in scrape-off region to eliminate plasma current outside separatrix.

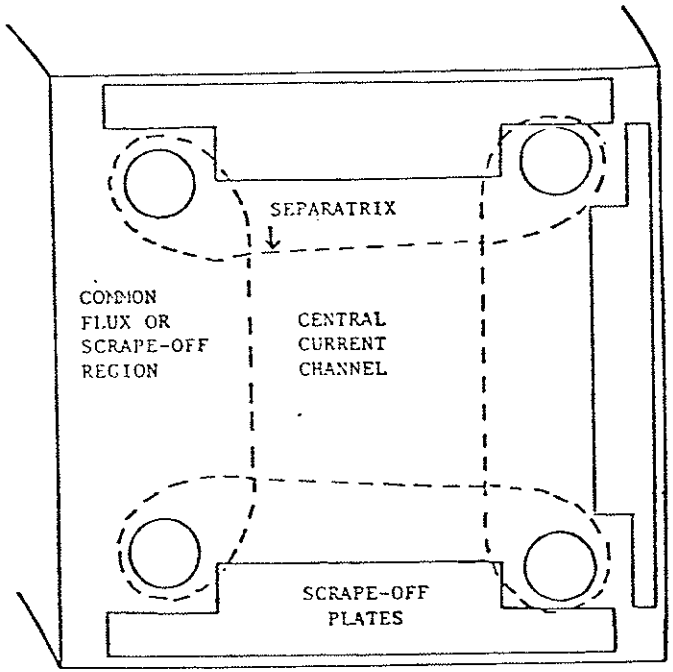

THE TOKAPOLE II DIVERTOR CONFIGURATION

Fig. 3-5: Time evolution of fields for Tokapole II discharge.

Maximum total hoop current, I_H, is typically 300 kA.

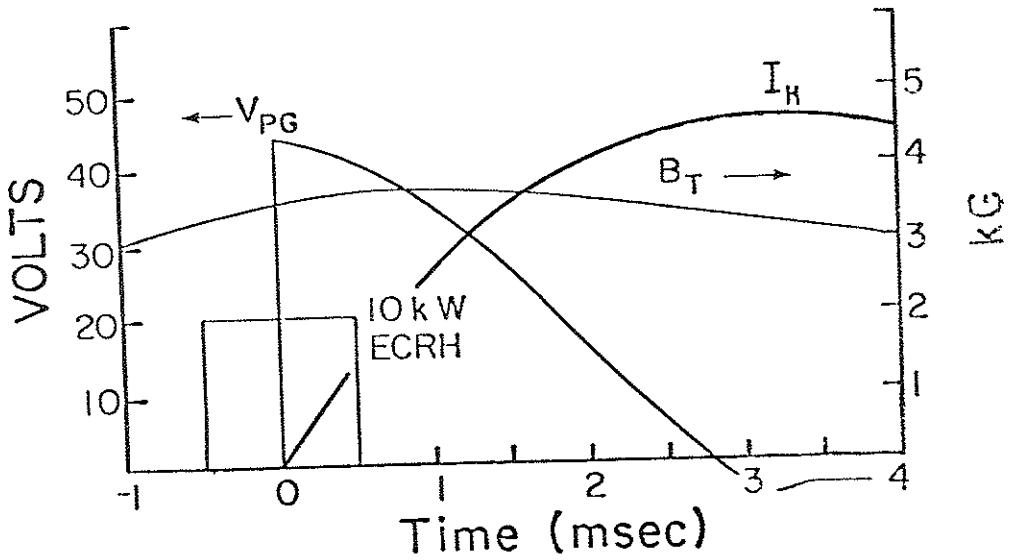
VOLTS
50
40
30
20
10
V_{PG}
I_K
B_T
10 k W
ECRH
5
4
3
2
1
kG
-1
0
1
2
3
4
Time (msec)

approximately constant toroidal field during the duration of the discharge. The poloidal gap voltage is power crowbarred to extend the length of the discharge up to a maximum of about 15 msec. Preionization is provided by 10 kW of either K-band (16.5 GHz) or X-band (9.0 GHz) microwaves depending on the toroidal field strength used. This produces a low density start-up plasma which seems to give a more reproducible discharge than would result from relying on avalanche breakdown alone.

There are two general types of discharges that have been used in these experiments. One is a relatively high current, high density discharge (but of shorter duration), while the other is a relatively lower current, lower density discharge but with a longer duration with several milliseconds of quasi-steady state (without probes inserted past the separatrix). The primary difference in the production of these two types of discharge was the presence of a "damping" resistor in the primary circuit of the transformer driving the plasma current.

Figure 3-6a,b shows current and density traces for the two types of discharge. The dashed traces are the typical results when a magnetic probe is placed several centimeters inside the separatrix. Note that the "normal" Tokapole II discharge, i.e. the longer lasting one is effected considerably more than the shorter discharge type. For considerably more detail

Fig. 3-6: Current and line average density waveforms for high current discharge (a) and for lower current "normal" Tokapole discharge (b). The dashed lines represent the typical effects of probes when inserted a few centimeters within the separatrix.

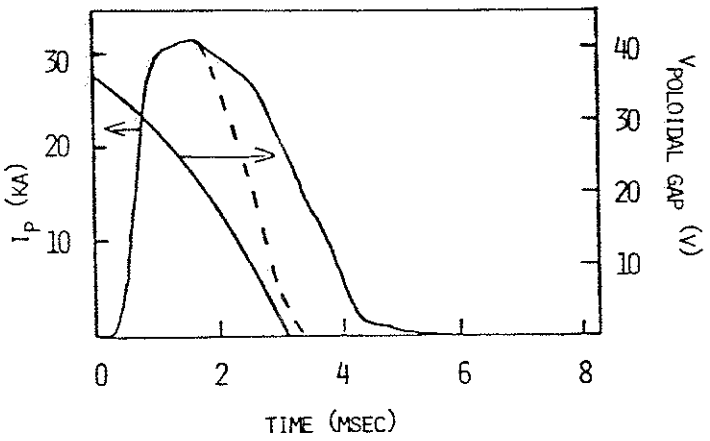
30
20
10
I_p (KA)
40
30
20
10
$V_{POLOIDAL\ GAP}$ (V)
0
2
4
6
8
TIME (MSEC)

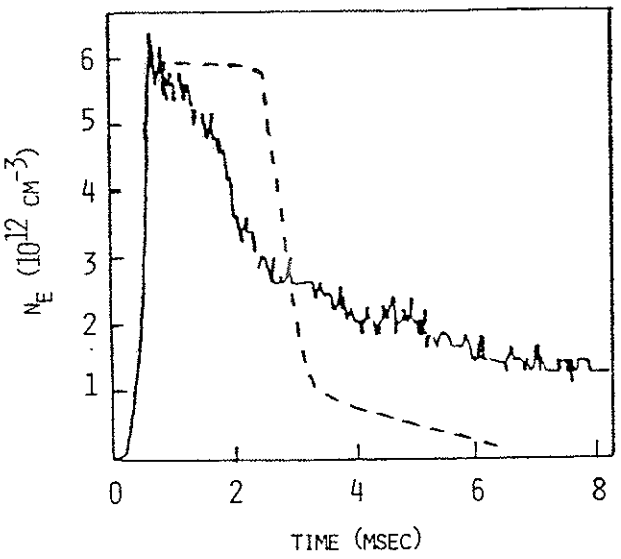
6
5
4
3
2
1
N_E (10^{12} CM^{-3})
0
2
4
6
8
TIME (MSEC)

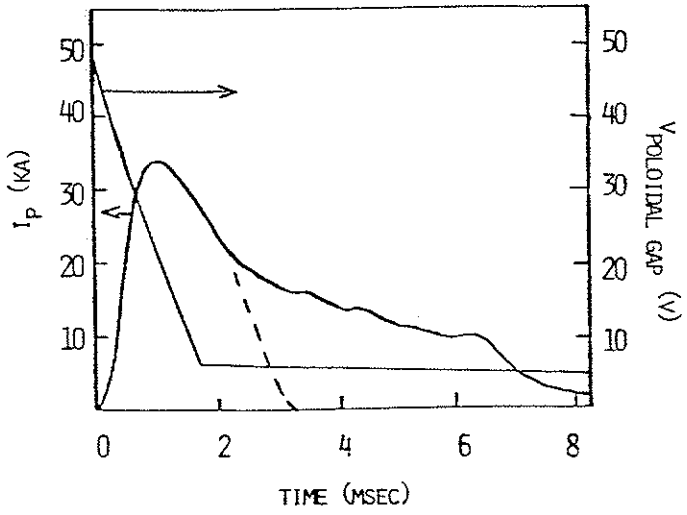
50
40
30
20
10
I_p (KA)
50
40
30
20
10
$V_{POLOIDAL\ GAP}$ (V)
0
2
4
6
8
TIME (MSEC)

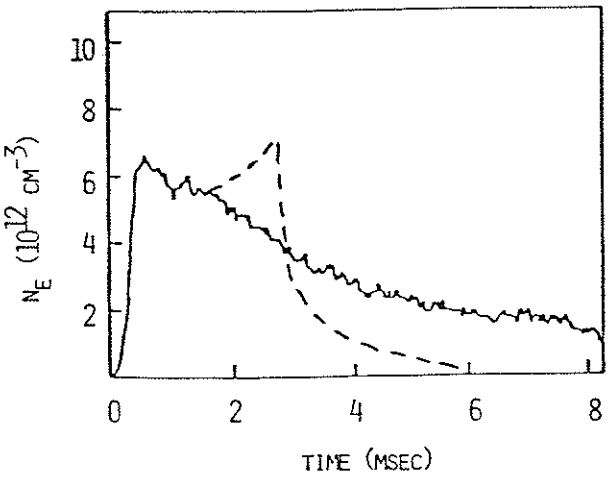
10
8
6
4
2
N_E (10^{12} CM^{-3})
0
2
4
6
8
TIME (MSEC)

concerning Tokapole II discharges, see the theses by Brickhouse[11] and Osborne[7].

Table 3-1 gives a summary of typical Tokapole II parameters.

TABLE 3.1 TOKAPOLE II PARAMETERS

Major radius	50 cm
Minor radius of plasma	6-10 cm
Toroidal magnetic field	~8 kG
Plasma current	10-40 kA
Line average density	$2\text{-}10\times10^{12}$ cm^{-3}
Electron temperature	~100 eV
Ion temperature	~20 eV
Energy confinement time	500-1000 μsec
Discharge length	3-15 msec
Base vacuum	$\sim3\times10^{-7}$ Torr

REFERENCES - CHAPTER 3

1. A.P. Biddle, et al., Nucl. Fusion 9, 1509 (1979).

2. J.C. Sprott and T.W. Lovell, University of Wisconsin PLP 744 (1978).

3. R.J. Groebner, Ph.D. Thesis, University of Wisconsin (1979).

4. L. Oren and R.J. Taylor, Nucl. Fusion 17, 1153 (1977).

5. H.F. Dylla, S.A. Cohen, S.M. Rossnagel, G.M. McCracken, and Ph. Staib, "Glow Discharge Conditioning of the PDX Vacuum Vessel," presented at the 26th National Symposium of the American Vacuum Society, New York (1979).

6. B.Lipschultz, Ph.D. Thesis, University of Wisconsin (1979).

7. T.H. Osborne, Ph.D. Thesis, University of Wisconsin (1984).

8. L.A. Artsimovich, Nucl. Fusion 2, 215 (1972).

9. H.P. Furth, Nucl. Fusion 15, 487 (1975).

10. J. Sheffield, Proc. IEEE 69, 885 (1981).

11. N.S. Brickhouse, Ph.D. Thesis, University of Wisconsin (1984).

CHAPTER 4

RF APPARATUS

4.A. Launching structures

4.A.1. Ideal launching structure

As pointed out in Chapter 2, the mode we wish to study for heating purposes is helical in nature. According to ideal MHD, the best way to drive a helical mode is with a helical antenna wrapping around the tokamak current channel with the same pitch as that of the mode. For the experiments on Tokapole II, such an antenna was completely out of the question for two reasons. First, a helical antenna would severely interfere with the many other experiments on Tokapole II. And secondly, even if there were no other experiments, it is not really possible to use a helical antenna in Tokapole II because of the divertor rings. It could not be placed outside the divertor rings because it would then link the rings, which is unacceptable for electrical reasons, and since the antenna would then be far from the plasma. Neither could it be placed inside the minor radius of the divertor rings, because proper plasma formation would then be interfered with, preventing a good equilibrium. We were thus forced to consider other possibilities.

The next best choice to a helical antenna is an array of separate and distinct loop antennas distributed about the current channel in such a fashion that, with proper phasing of the rf currents in each of the antenna loops, one obtains a step approximation to a helical antenna. The idea is illustrated in Figure 4-1. Basically, what one is doing is simply to cut out small sections of the helical antenna and then force each of these sections to carry the same current and phase it would have carried had it still been part of the original helical antenna. Obviously, the more sections used, the better the approximation to a helical antenna. But this also increases the complexity of the external driving circuitry required, since each section needs to be carefully phased with respect to the others.

In principle, if one is concerned mainly with the lowest order poloidal and toroidal modes, with mode numbers m and n respectively, then the minimum number of antennas needed for effective coupling is four. These would be distributed as two sets, with two antennas per set. Each set would be separated by 180° toroidally, and by 180° poloidally within each set. By driving these antennas either in or out of phase, one then preferentially couples to the modes (m,n)=(1,1), (1,2), (2,1), (2,2). Of course, a spectrum is actually generated, but most of the power will go into the lowest modes.

This kind of antenna system was rejected, temporarily at

Fig. 4-1: Finite section approach to a helical antenna. By operating all antennas in phase, coupling to the helical field line is obtained. Best coupling is obtained when each antenna is rotated so that it is locally parallel to the field line.

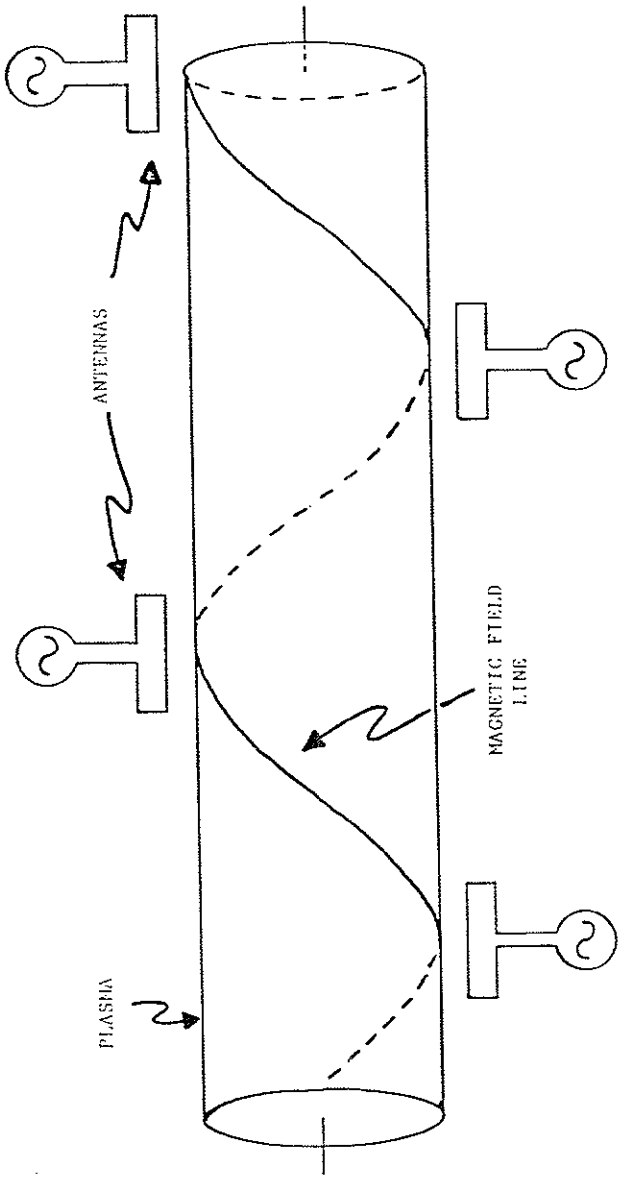

least, because it was desired to begin the experimental phase immediately, and the design and fabrication of new antennas would take some time. It was possible to make this decision at the start, because there existed another possibility for an antenna which already happened to exist. This third possibility was to utilize the divertor rings themselves as the launching structure. As will become clear, this was only an interim solution to allow experimental work to begin quickly and not the ultimately desired launching structure.

4.A.2. Divertor ring antenna

The basic idea is straightforward and is illustrated in Figure 4-2. Each divertor ring has three conducting support rods which are electrically insulated from the vacuum vessel. These supports provide the means to superpose rf currents on top of the inductively driven equilibrium "dc" currents present during the plasma discharge. What is desired is to set up an rf current distribution that has a toroidal mode structure. This can be done with the hoops simply by grounding one of the hoop supports to the vacuum vessel and driving one of the remaining supports from a source of rf power. The third support is left floating and unused in this configuration. The ring effectively acts as an inductor at rf frequencies. The resulting toroidal current distribution is plotted in Figure 4-3. Note that current flows in both toroidal directions, thus

Fig. 4-2: Toroidal mode generation of divertor ring antenna.

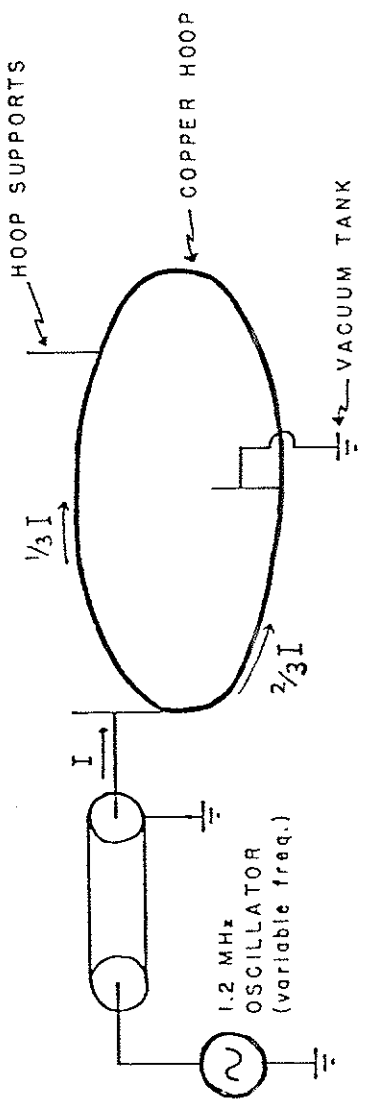

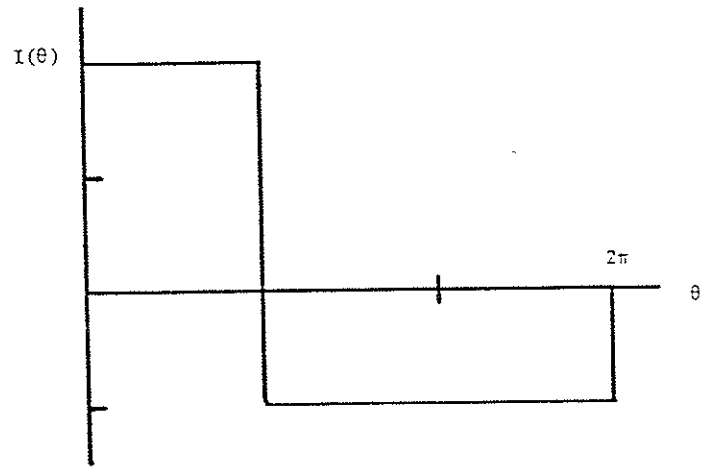

Fig. 4-3: Toroidal current distribution for divertor ring antenna. Fourier analysis yields a spectrum of toroidal mode numbers with amplitudes decreasing as 1/n. Multiples of three are absent from the spectrum due to the symmetry.

setting up a toroidal mode structure. Fourier analysis of this current distribution indicates a broad spectrum of toroidal modes but with Fourier amplitudes falling off as 1/n. Thus greater than 75% of the total power goes into the two lowest modes, n=1 and 2. Due to symmetry, mode numbers which are multiples of three are not present.

The establishment of a poloidal mode structure is indicated by Figure 4-4. For instance, an m=4 configuration is established by driving all four rings in phase with each other. Because of the geometry of the hoops, the rf currents actually fight against the helical mode for some sections of toroidal azimuth. In spite of this though, there is a weak coupling to helical modes.

There is one other method of driving the hoops which is more appealing from a symmetry point of view. That is to ground two supports while driving the remaining one. This would drive equal rf currents in opposite direction in two legs of the hoop while allowing zero current between the two grounded supports. In principle, this is a superior antenna than the single ground approach. Unfortunately, two supports cannot be directly grounded simultaneously because of the perturbations this would have on the equilibrium currents of the hoops. To get around this, we attempted to place the two supports at "ac" ground through capacitors which were a high impedance at the 100 Hz frequency of the equilibrium currents,

Fig. 4-4: Poloidal mode generation for divertor ring antenna. m=4 combination is shown. Generation of m=1 or 2 is accomplished by driving opposite rings either out of or in phase respectively.

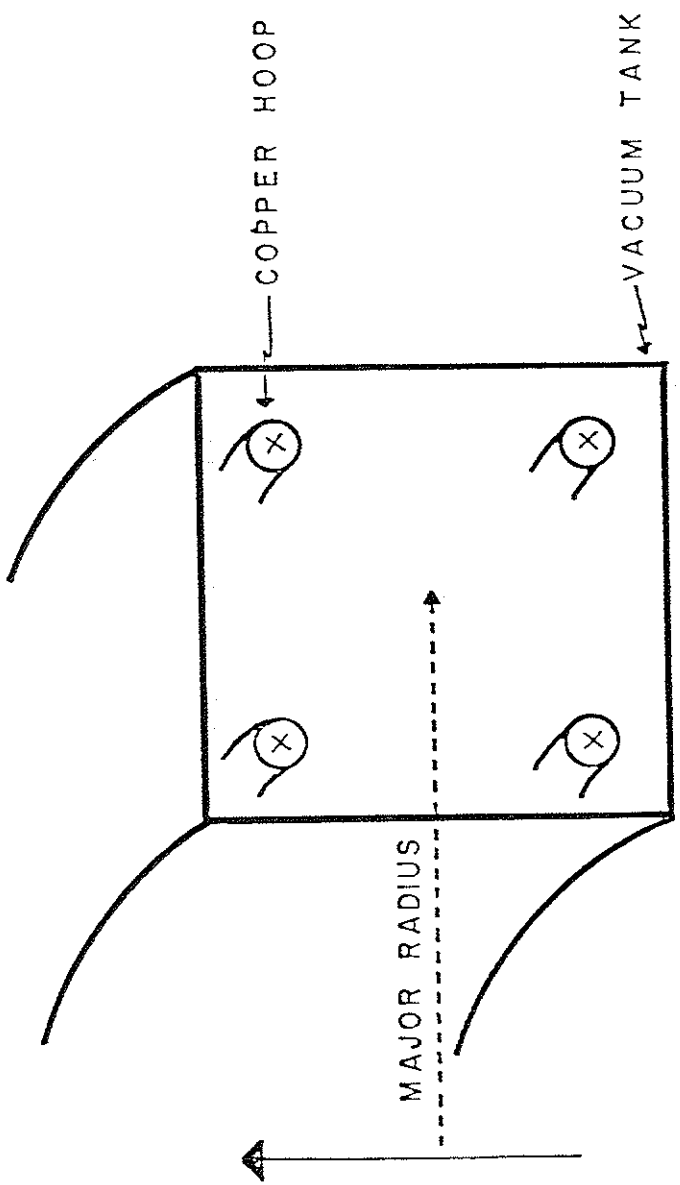

yet a small impedance at 1 MHz. This does not work very well, though, due to the extreme sensistivity of the circuit to resonant effects with the 1/3 of the ring between the "grounded" supports, and to unavoidable stray leads. It was necessary to abandon this technique for the much simpler single ground approach.

As the circuit of Figure 4-2 stands, it would be difficult to drive much rf current through the rings because of their low impedance. The situation is vastly improved by placing capacitance across the rings forming a resonant LC "tank" circuit. By choosing the capacitance to resonate the effective hoop inductance at the frequency of the rf source, the circulating current through the rings can be increased by a factor equal to the circuit Q. For the hoops this turns out to be ~20 in vacuum. This also provides a roughly constant purely resistive load to the rf source, as opposed to a low impedance inductance. The equivalent circuit for a ring is shown schematically in Figure 4-5. The equivalent circuit for an m=4 configuration is shown in Figure 4-6. At 1.2 MHz, an m=4 configuration presents a 50 Ω load to the rf source.

Probably the most serious problem encountered in this experiment has been the need to measure magnetic probe coil output signals of a few tens of microvolts in an extremely high rf noise environment. There are two approaches one can follow in trying to eliminate this noise from the measurement system.

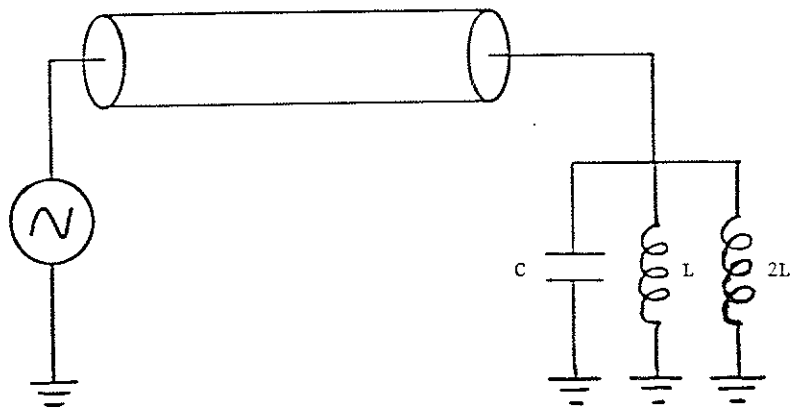

Fig. 4-5: Equivalent circuit for a single ring with resonating capacitor. L and 2L represent the inductances of the two legs of the ring.

Fig. 4-6: Equivalent circuit of m=4 configuration. Coaxial transmission lines (RG/8) from single feed line to each ring have been left out of figure for clarity.

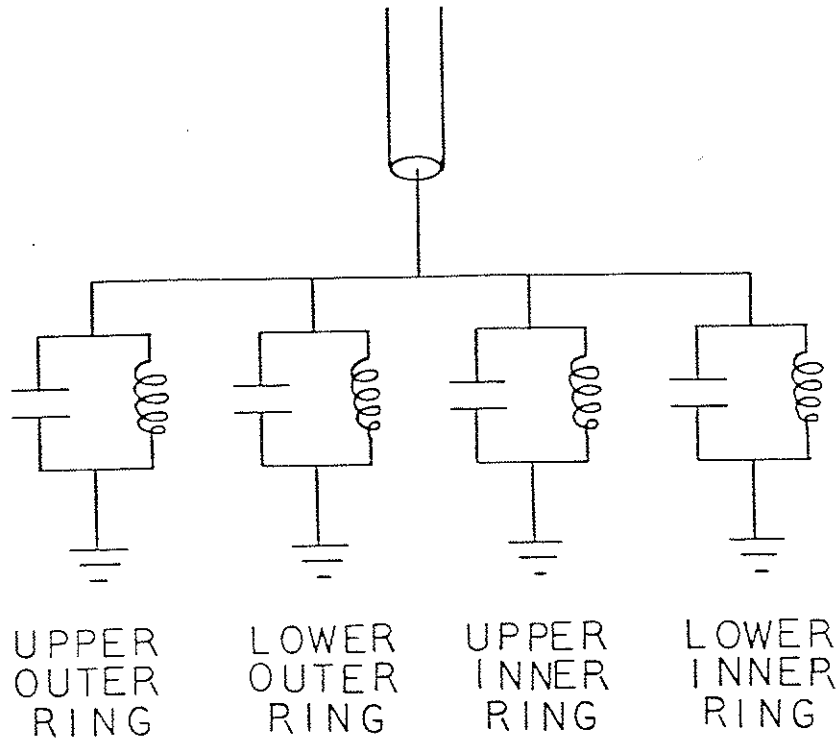

One is to shield the measurement system, which will be discussed in Section 4.C. The second is to shield the original source of the rf noise, i.e. the oscillator, transmission lines and antenna. Since neither of these techniques is 100% effective, a combined approach was found to be necessary.

Shielding the source of rf noise consists of placing an electrostatic shield around the entire rf generation system. This includes the pulse forming network, the oscillator, the transmission lines and as much of the antenna as possible. Since an antenna has the purpose of radiating rf energy, it is clear that perfect shielding is impossible. The task is to confine the rf only to the interior of this shield and thus prevent it from coupling to circuits in other parts of the room. A schematic of the arrangement that eventually worked can be found in Reference 1.

In order to avoid ground loops, which can cause as much pick-up problem as direct radiation, the electrostatic shield is grounded to the oscillator circuit ground and insulated from the Tokapole II tank which is the normal experiment ground. Copper screen mesh imbedded within a fiberglass matrix cast in the form of a "hat" covers the electrical connections to the hoops. (Schematics of this system can be found in Reference 1.) This area was identified as one of the worst radiators of the entire system due to the unavoidably large loop involved with the electrical connection to the ring supports, and due to

the proximity of this loop with its large circulating rf currents to the magnetic probes. Spurious ground loops which occur randomly can still cause significant pick-up problems if not eliminated. The rf power to the antenna is also inductively coupled from the oscillator to avoid ground loops as shown in the figure. The series resonant circuit shown in the transmission line was necessary to remove harmonic noise from the drive voltage. For more details concerning the divertor ring launching structure see Reference 1.

4.A.3. The New antenna

4.A.3.a. Reasons for a new antenna

Before describing the new antenna, let us first establish the reasons why the hoop antenna system is inadequate for future studies. These reasons provide the design rationale for the new antenna. The purpose of future studies will be focused on two aspects: more detailed study of the resonance structures and actual heating experiments. The hoop antenna system is inadequate for properly fulfilling either of these goals for the following reasons.

1) The divertor rings are not Faraday shielded and thus suffer severe electrostatic loading during a discharge due to the plasma in the private flux region around each hoop. This

lowers the Q and the parallel impedance of the resonant circuit, which are already quite low to begin with, and this in turn reduces the amount of circulating current available to drive the resonance. This reduced power delivery limits the size of the resonant magnetic field. Because of plasma generated rf noise in the frequency range that is being studied, and which cannot be filtered out without also removing the real signal, this complicates measurement of resonance properties. This has been a constant problem in this experiment, and it appears that the only solution to this particular problem is to increase the amplitude of the wave magnetic field by. Presumably, this will be possible with larger antenna current and a better coupling structure.

The original intent of the divertor scrape-off plates was to reduce the plasma near the hoops in the hope of reducing the electrostatic loading, and thus allow larger hoop antenna currents. Although the baffles succeeded in eliminating plasma current in this region, plasma density still remains quite high[2] (a few 10^{12} cm^{-3}), and electrostatic loading remains essentially unaffected. Since the parallel impedance of the hoops at resonance is very low (~50 Ω), this means the parallel equivalent impedance of the plasma would need to be quite low in order to couple significant power to the plasma. This would require at the very least a closely coupled antenna, which the hoops clearly are not.

2) A brute force approach to overcoming the electrostatic loading and low Q and $R_{\|}$ of the rings is not possible due to the low breakdown voltages that would be encountered in the ring support region when plasma is present.

3) From a physics point of view, one desires the simplest possible antenna which can excite the modes under study. The hoops have a very complicated mode structure with rf currents flowing in uncontrolled directions in the vacuum vessel walls, which act as the ground return. Not only does this complicate physics issues, but it also causes more noise pick-up problems because of the fields generated by these stray currents. As mentioned earlier, the hoops actually fight against the very modes they are supposed to be coupling to in certain parts of the toroidal extent. Obviously, this is an undesirable complication. It is highly desirable to be able to couple preferentially to either the n=1 or n=2 toroidal mode numbers without having a strong coupling to the other one at the same time. With the hoops, however, the toroidal mode structure is fixed and must be lived with.

4) One of the big questions of SARH is concerned with what is the optimal antenna (see Section 5.F). The question deals primarily with the direction of the antenna currents with respect to the ambient magnetic field (the physics of this will

be discussed in Chapter 5). To study this question experimentally requires an antenna whose orientation can be varied. The hoops do not have the capability to address this question.

5.A.3.b. Description of new antenna.

A new antenna was designed to overcome the many shortcomings of the hoop antenna and to extend the scope of possible studies at much higher power levels. The basic design follows that of the "next best design" from Section 4.A.1. A schematic diagram of the antenna is shown in two views in Figure 4-7. The antenna itself is simply a double series loop of solid copper bar. This double loop sits in a curved copper tub with the top enclosed by a Faraday shield. The purpose of the tub is to eliminate any change in inductance as the antenna is extended further into the vacuum chamber and away from the wall. This eliminates the need to retune after each antenna psoition change. It also increases the field above the antenna by roughly 50%. The Faraday shield prevents electrostatic coupling between the antenna and the plasma. The entire loop is curved to follow the toroidal direction. This keeps all parts of the antenna close to the plasma current channel and thus provides coupling over a larger plasma surface area.

The physical size of the antenna is such that it does not interfere with any future octupole studies that may be

Fig. 4-7: (a) End-on cross section view of high power antenna with representative rf magnetic field line.

(b) Schematic drawing of antenna currents indicating toroidal curvature of antenna.